

## Surface Flow Visualization

### Organization:

This document is organized as follows: (1) image acquisition procedures are discussed, (2) the surface flow visualization topography is presented and discussed for Cases A, B, and C, and (3) additional representative surface flow visualization images are included in the appendix for Cases A, B, and C. Note, for more details on the surface flow visualization and its interpretation via topological analysis, see Simmons et al [1] and Simmons [2].

### Acquisition Procedures:

Many variations of oil-film surface flow visualization were tried in this study, with the most useful being the kerosene and titanium dioxide approach in combination with the aviation oil and kerosene approach. This new approach was inspired by a recently-developed method from NASA Langley [3] where they used aviation oil, kerosene and nanosized fumed silica particles. The final recipe used here consists of: (67%) kerosene, (20%) w100 aviation oil, (12%) titanium dioxide and (1%) oleic acid all combined by weight and applied to the surface via lightly brushing. Aviation oil fluoresces under ultraviolet (UV) light, leaving luminous flow patterns on the surface. It was found that the titanium dioxide, with the addition of oleic acid to prevent clumping, aids the aviation oil in enhancing the surface skin friction lines.

The basic theory is that when a light coating of the mixture is applied to the surface and a shear is applied by running the wind tunnel, the kerosene acts as a carrier agent and allows the aviation oil and titanium dioxide to flow along the surface. The air flow accelerates the evaporation of kerosene, which ultimately leaves behind the titanium dioxide powder and aviation oil. Since the layer of oil on the surface is thin, it retains the surface flow pattern with plenty of time to stop the tunnel, apply a UV light, and photograph the final steady-state results.

The procedure used in the oil-film surface flow visualization studies was as follows. First, the ramp surface was cleaned to remove any residue. Next, a flexible, adhesive-backed measuring tape was placed over the centerline pressure ports. This serves as both a fiducial marker and prevents the oil mixture from clogging the ports. The oil mixture was then thoroughly mixed to keep the titanium dioxide particles from sinking to the bottom. A thin coat of this mixture was brushed on surface. After this, the removable tunnel window was bolted in place and the wind tunnel was quickly turned on to the desired speed of Mach 0.2. In most cases, the test duration was approximately 30-60 minutes, which allowed most of the kerosene to evaporate. After stopping, the window was removed and a custom UV light booth, shown in Figure 1.b, was placed above the ramp. Finally, multiple photographs were acquired using a Canon Rebel t6 camera featuring a resolution of 5184 x 3456 pixels.

In some of the surface flow visualization studies, a video camera was placed in the test section to record the development of the surface flow patterns. This camera was a 5-megapixel, HD lipstick camera featuring a CMOS image sensor and a 3.6 mm wide angle lens. The camera was mounted to the central section of the downstream diffuser cruciform as shown in Figure 1.a.

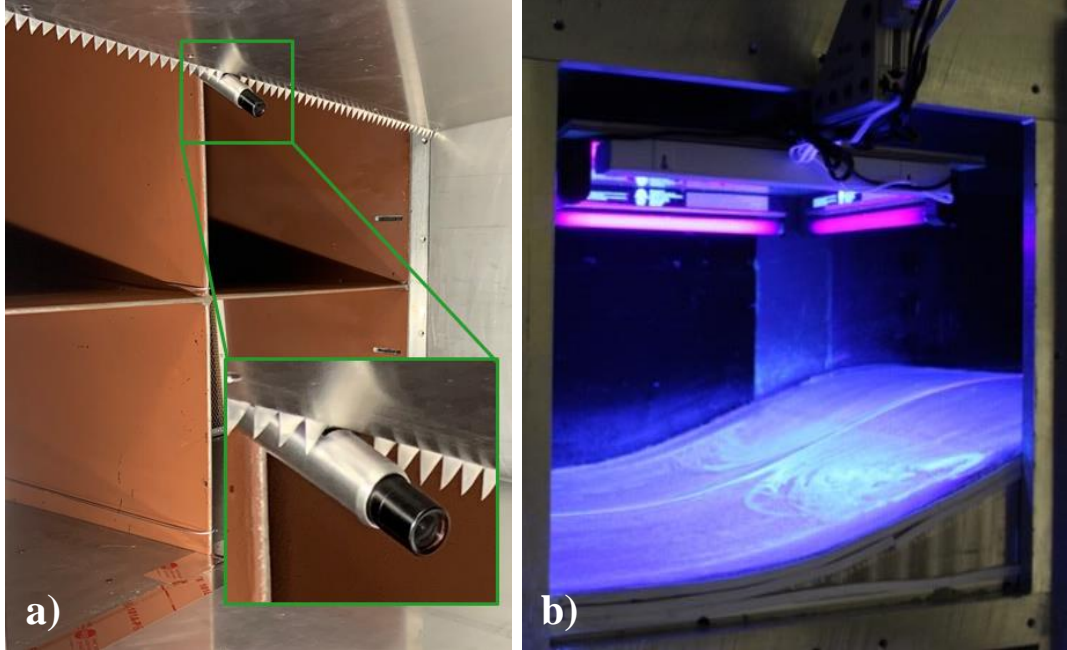


*Figure 1 Photographs of, a) the diffuser mounted video camera, and b) the UV light fixture installed and illuminating the ramp surface flow.*

## Surface Flow Visualization

### **Case A**

The detailed topography of the surface flow pattern for the large-scale separation case, Case A, is presented here. For a more complete description and analysis of flow separation topography and topology see Simmons et al. [1]. The global surface flow visualization, consisting of the pattern of skin-friction lines, is presented in Figure 2. The surface flow pattern is clearly dominated by the presence of two large, symmetric, counter-rotating vortical structures in the central region of the ramp and a spanwise uniform reattachment location farther downstream; together these structures extend over approximately 50% of the ramp surface. The surface flow pattern over the majority of the ramp is inherently three-dimensional. The flow approaching the ramp from the boundary layer development plate is two-dimensional in nature, except very near the sidewalls where the presence of the boundary layer retards the flow. Once the flow starts to pass over the ramp, the presence of the adverse pressure gradient and/or wall curvature begins to morph the flow into a seemingly complex three-dimensional structure that exhibits a considerable degree of side-to-side symmetry with respect to the spanwise center plane.

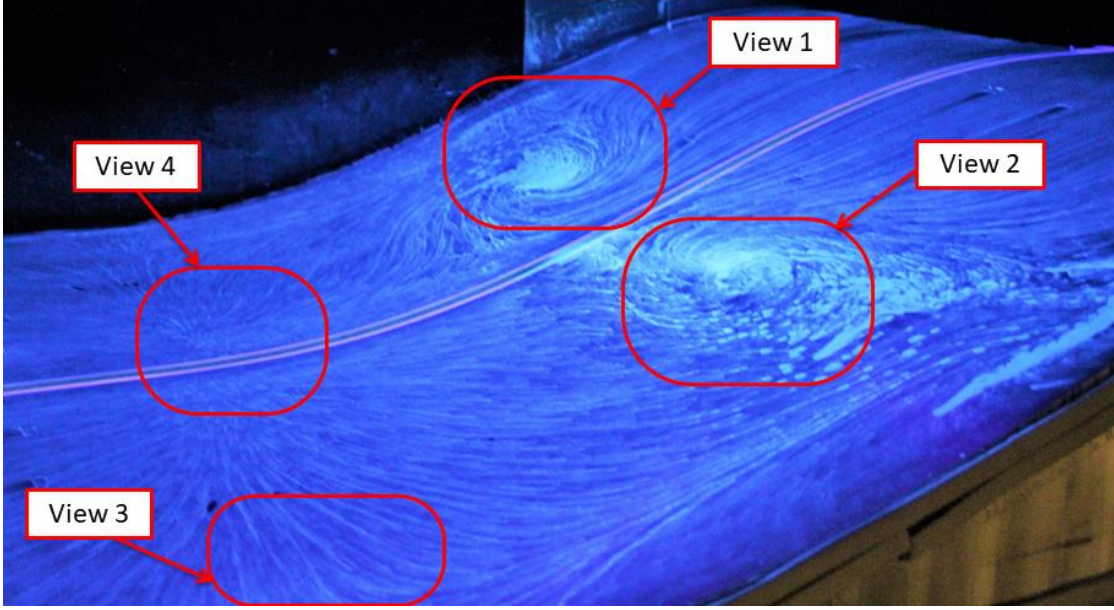


Figure 2 Global surface flow visualization for Case A, with four interrogations regions highlighted. Incoming flow is from right to left

Due to the large spatial extent of the ramp geometry and the detailed surface flow features, four interrogation regions will be presented in more detail and described separately before a global analysis of the entire ramp surface will be presented. View 1 of Figure 2 is highlighted in Figure 3. This figure presents the surface detail of the separation structure and surrounding smaller-scale flow topography on the far side (inner loop side) of the wind tunnel. Note that there are two prominent saddle points. Along the centerline, the flow is drawn toward saddle point 1 (S1), whereas the flow nearer the sidewall is drawn toward saddle point 3 (S3). Both saddle points then divert the flow into the central focus 2 (F2), where the flow must lift off of the surface due to the Helmholtz vorticity theorem (i.e. a vortex tube cannot end within a fluid). The line dividing the upstream region from the downstream region, shown as the yellow dashed line, is known as the global line of separation. The line of separation forms the base of the stream surface, which is called a dividing surface [4], where the flow detaches from the ramp. This dividing surface extends into the flow and advects downstream.

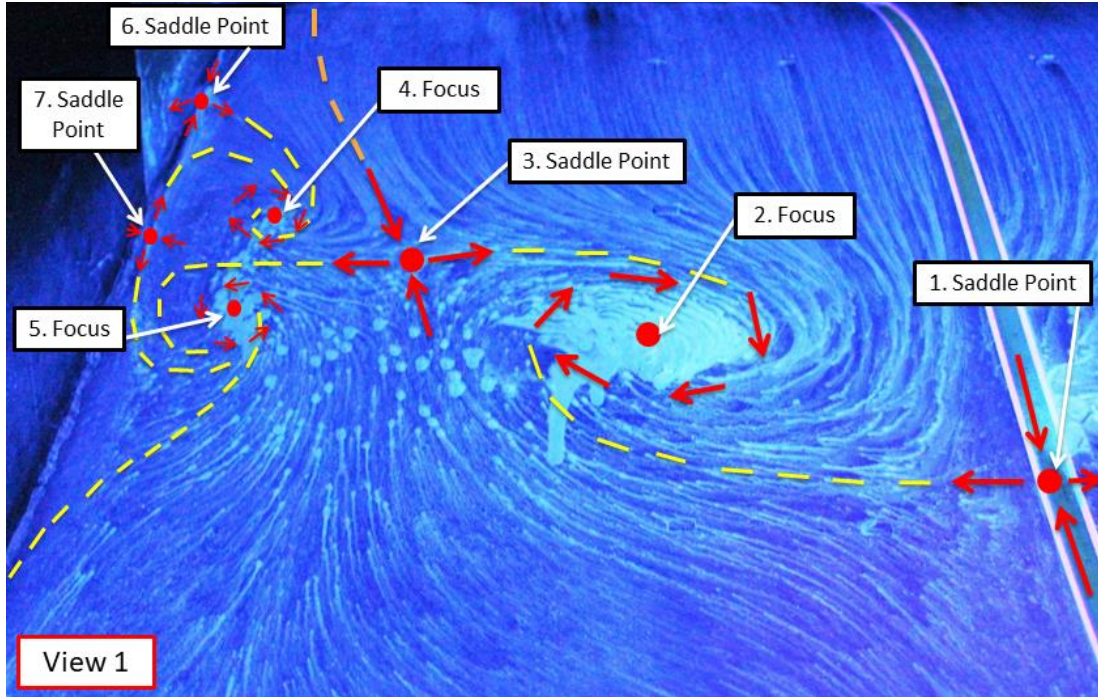


Figure 3 View 1, from Figure 2, with the yellow dashed line indicating separation and the orange dashed line showing how the near sidewall flow is topologically isolated from the central flow separation. Incoming flow is from top to bottom.

Nearer the tunnel sidewall, there are a number of smaller scale structures (also connected to the dividing surface just mentioned); two appear to be the counter-rotating foci, F4 and F5, which are bounded by two saddle points, S6 and S7, which are very near the sidewall. The farthest upstream saddle point, S6, appears to be the source of the sidewall separation. Its extent is limited by S3 as the skin-friction lines that were moving away from the sidewall are diverted back and around F4.

As was the case in View 1, shown in Figure 3, View 2, shown in Figure 4, presents the separation topography occurring on the near side (wind tunnel outer loop). Despite some small near-wall differences, globally, the centerline symmetry is very good. What is apparent from images taken on both sides of the tunnel centerline is that the sidewall separation, emanating from S6 and S16, is topologically isolated from F2 and F12 by S3 and S13; hence, from a skin-friction line point of view, the sidewall flow does not directly influence the central separation structures. This indicates that *sidewall separation is not the main cause of the formation of vortical structures on the ramp*. Instead, any direct influence the sidewall boundary layers have on the central vortical structures is limited to the area farther upstream, prior to the location where boundary layer separation occurs. While sidewall separation does not directly cause the central vortical structures, it does indirectly affect them.

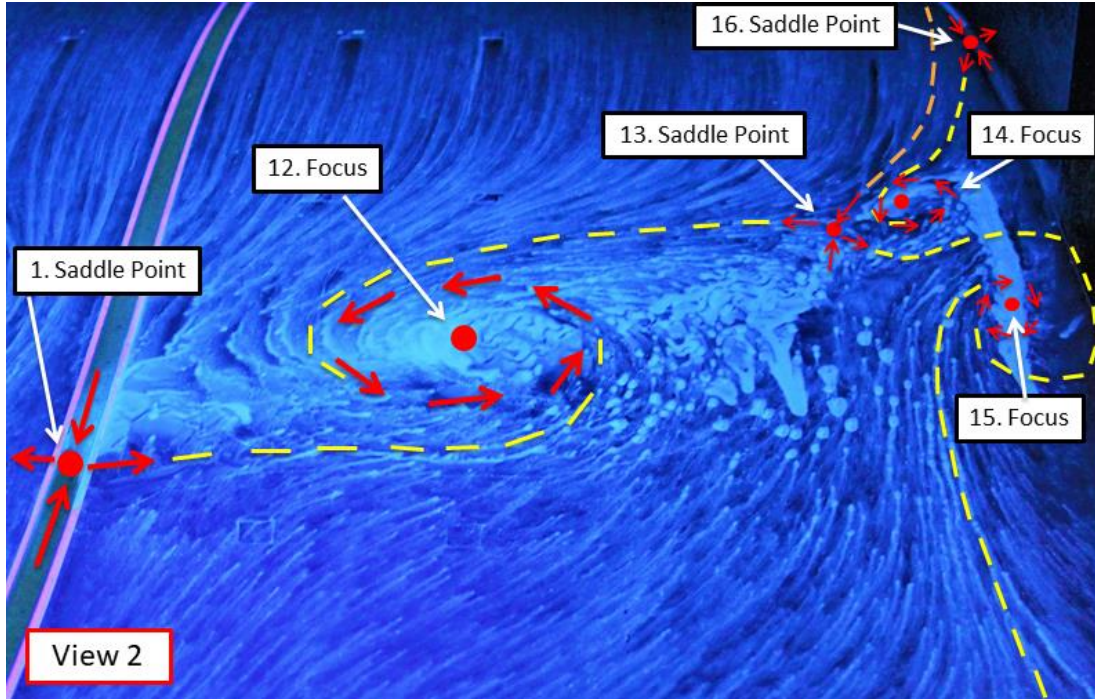


Figure 4 View 2, from Figure 2, with the yellow dashed line indicating separation and the orange dashed line showing how the near sidewall flow is topologically isolated from the central flow separation. Incoming flow is from top to bottom.

The reattachment region, which is highlighted in Views 3 and 4, is shown in Figure 5. While the separation region is three-dimensional, the reattachment is, in contrast, quite two-dimensional. This is highlighted by the red dashed line. Central reattachment initiates at node N22, which acts as a source, feeding in all directions with an almost pure crossflow component along the reattachment line. Just up or downstream of this line there is still a major crossflow component that appears to vary slightly with spanwise location, indicating some limited degree of three-dimensionality. As the flow approaches the near wall, it is redirected by saddle point S21, after which point the crossflow component changes direction. Another near-sidewall nodal source, N20, feeds into S21 as well as into the upstream focus F15. Note that due to the nearly perfect symmetry, the far wall topography is not presented here.

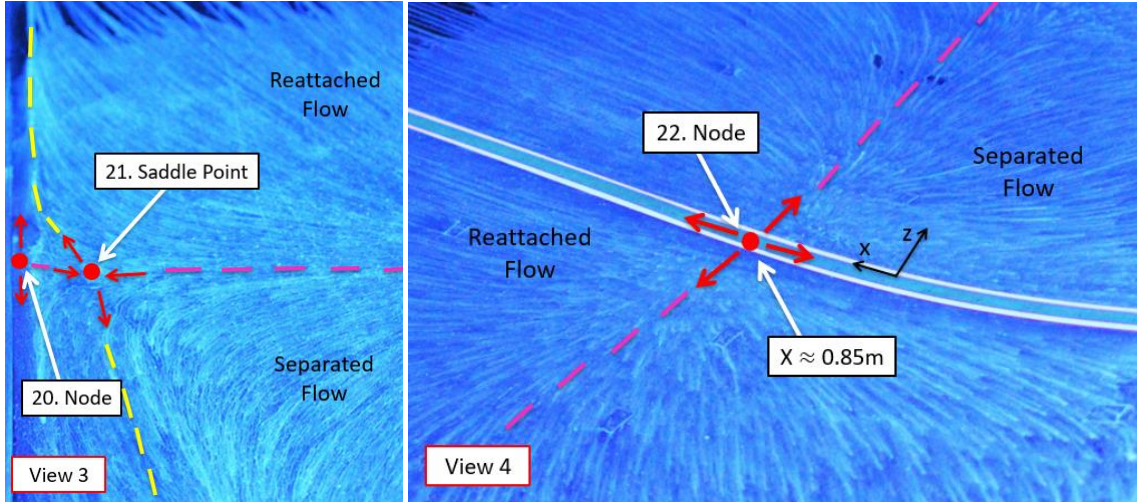


Figure 5 Close up views of the reattachment in the central ramp region (View 4) and near the wind tunnel outer loop sidewall (View 3). Incoming flow in both images is from right to left.

All the surface flow images shown in Figure 2, Views 1-4, were taken as part of a single wind tunnel run. Later, flow visualization was conducted on each sidewall to individually capture the associated topological features there. Close-up photographs were taken in-situ, as well as with the window insert removed. Figure 6 shows the surface flow visualization on the wind tunnel outer loop sidewall and highlights both the sidewall juncture flow separation and sidewall reattachment. Figure 6.b shows the initiation of separation from both the ramp surface and sidewall juncture. Both lines of separation initiate from saddle point S16 (see Figure 4) and terminate into foci F14 and F18. It is likely that in the flow above the surface, F14 and F18 are connected by the same stream surface spiraling into their cores. In essence, one vortex curves and impinges on the surface leaving “footprints”, F14 and F18, on the ramp and sidewall. Saddle point S17, which was not visible in Figure 4, is located on the sidewall. It is connected to F14, which was determined in additional flow visualization experiments that are not shown here.

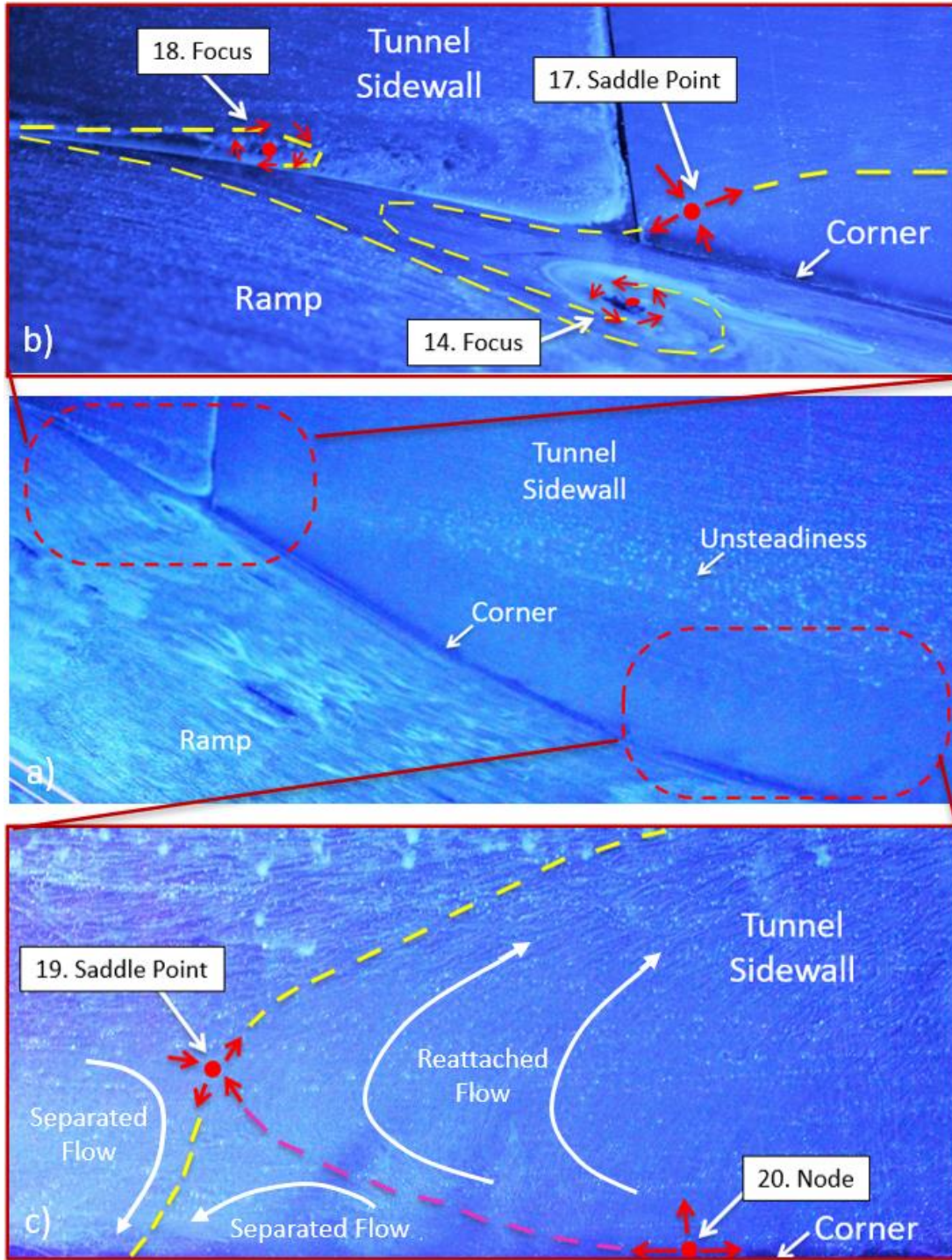


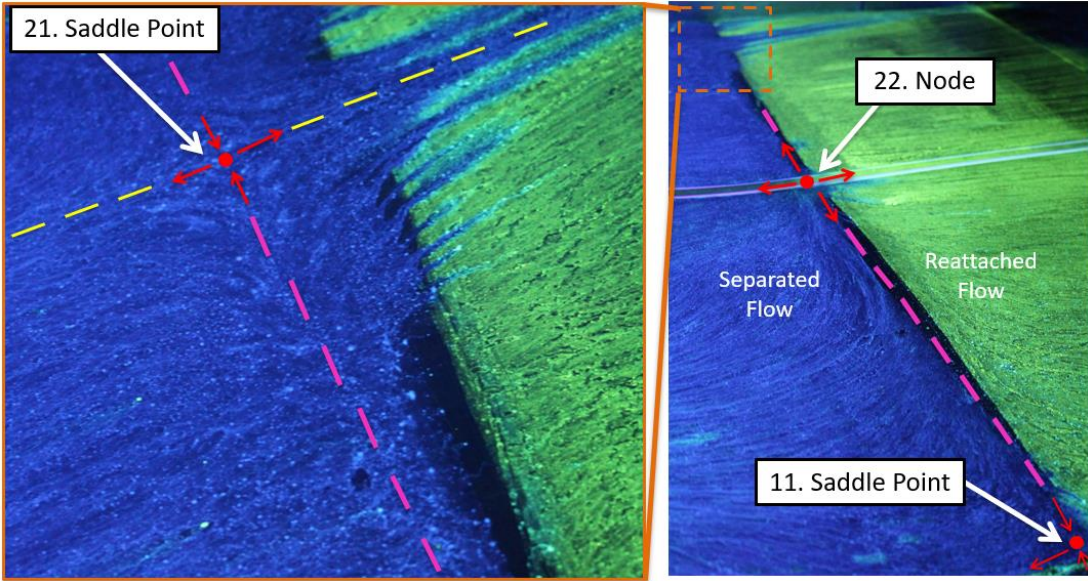
Figure 6 (a) Surface flow visualization on the ramp surface and wind tunnel outer loop sidewall, (b) with close up views highlighting the sidewall juncture flow separation and (c) sidewall reattachment. Incoming flow is from left to right in all images.

Figure 6.c highlights the reattachment region. The reattachment line on the surface of the ramp passes through N20, as also seen in Figure 5, and then leads up the sidewall surface into saddle point S19. Looking closely, one can see many reattached source lines leaving node N20

and heading upstream before being diverted back downstream by saddle point S19. This saddle point is the last singular point in the reattachment line and divides the separated flow, which heads upstream into F15 (see Figure 4) from the reattached flow, which heads downstream.

For this experiment to be well-suited for a benchmark CFD validation study, the repeatability of the previously described surface flow is a primary concern. To ensure a high degree of repeatability, numerous individual flow visualization runs were conducted each time the experimental setup was reinstalled or altered. Furthermore, many flow visualization techniques were implemented, utilizing varied solution fluid viscosities. This was done to minimize the effect of pressure/gravitational forces and to capture the best representation of the actual surface flow pattern which is important for revealing the underlying topological features of the surface flow.

One such variation in method was to use two solutions that would illuminate in different colors under UV lighting. The base solution, which emitted light in a blue color, was the same aviation oil solution described in the acquisition procedures, while a different solution consisting of kerosene, silicone oil and UV leak detection dye, emitted light in a bright green color. The primary advantage of using two different colored solutions was that the distinction of the various flow regions could be emphasized in more detail. For example, the reattachment of the flow is highly two-dimensional and repeatable. To highlight this, Figure 7 shows a test run where the blue solution was placed in the separated flow region and the green solution was placed just downstream from the reattachment region. After approximately an hour of run time, the wind tunnel was stopped, and the results were photographed. Remarkably, there is almost no mixing of the two solutions, thereby indicating the temporal stability of the flow reattachment pattern. Where the blue dye is placed, almost all the flow is reversed, characteristic of the separation region. In contrast, where the green dye is placed, all the flow is directed downstream, characteristic of attached flow. The only region where mixing occurs is on the far side where the reattachment line is biased slightly upstream from where the blue dye was placed and hence the flow diverted by S21 can be clearly seen heading downstream.



*Figure 7 Two-dimensionality of the reattachment region, captured using two different UV illuminating surface flow solutions. Note that incoming flow is from left to right in both images.*

The oil-film flow visualization is a very sensitive diagnostic tool. The dramatic mixing of the blue dye near S21 shows just how much surface movement in the fluid occurs. Furthermore, this mixing is only apparent since the blue dye was initially applied just over the reattachment line, highlighting just how remarkably spanwise uniform the reattached flow is. The surface flow separation pattern was very repeatable run-to-run. However, unlike reattachment, the separation process seems to be quite sensitive to upstream flow conditions. Due to this sensitivity, great care was necessary in the test section installation process to ensure that the flow conditions did not change.

#### Case B

The global surface flow visualization for the smaller-scale separation case, Case B, is shown in Figure 8. This image also includes flow visualization of the far sidewall. Many of the topological features of this case are quite similar to those occurring in the larger-scale separation case, Case A, and therefore will not be discussed in detail. Instead, the focus of this section will highlight the important similarities and differences between these two cases. The primary vortical flow patterns in the central region are still prominent, remain spanwise symmetric, and exhibit a significant degree of three-dimensionality.

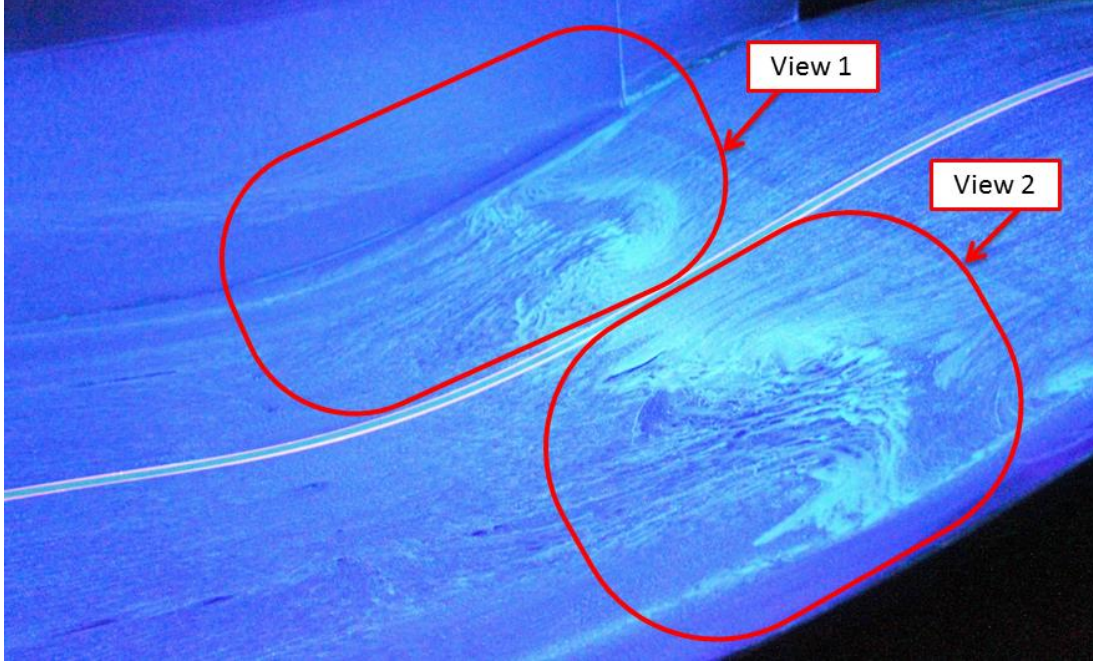


*Figure 8 Global surface flow visualization for the small-scale separation, Case B, highlighting two viewing regions to be analyzed in greater detail. The incoming flow is from right to left.*

Figure 9 shows a detailed view of the topological features within View 1 of Figure 8. The topography and topology of the global line of separation are approximately the same here as they were in Case A. The most notable difference is in the topology of the reattachment line where an extra pair of singular points, saddle point S23 and node N24, are present. Both of these features terminate in focus F5 and do not appear to affect the two-dimensionality of the reattachment line. Centerline symmetry is also maintained with the addition of an extra pair of singular points, saddle point S25 and node N26, on the near side reattachment line, as shown in Figure 10, View 2. This near side view also highlights the improved centerline symmetry in the global line of separation, as compared to Case A. Here saddle point S13 is located farther from the sidewall, balancing the centerline symmetry with saddle point S3 (Figure 9). In light of this, Views 1 and 2 show the distinct central flow leading into saddle points S3 and S13 (the orange dashed lines) demonstrating that the central three-dimensional flow separation pattern is isolated from the sidewall separation.

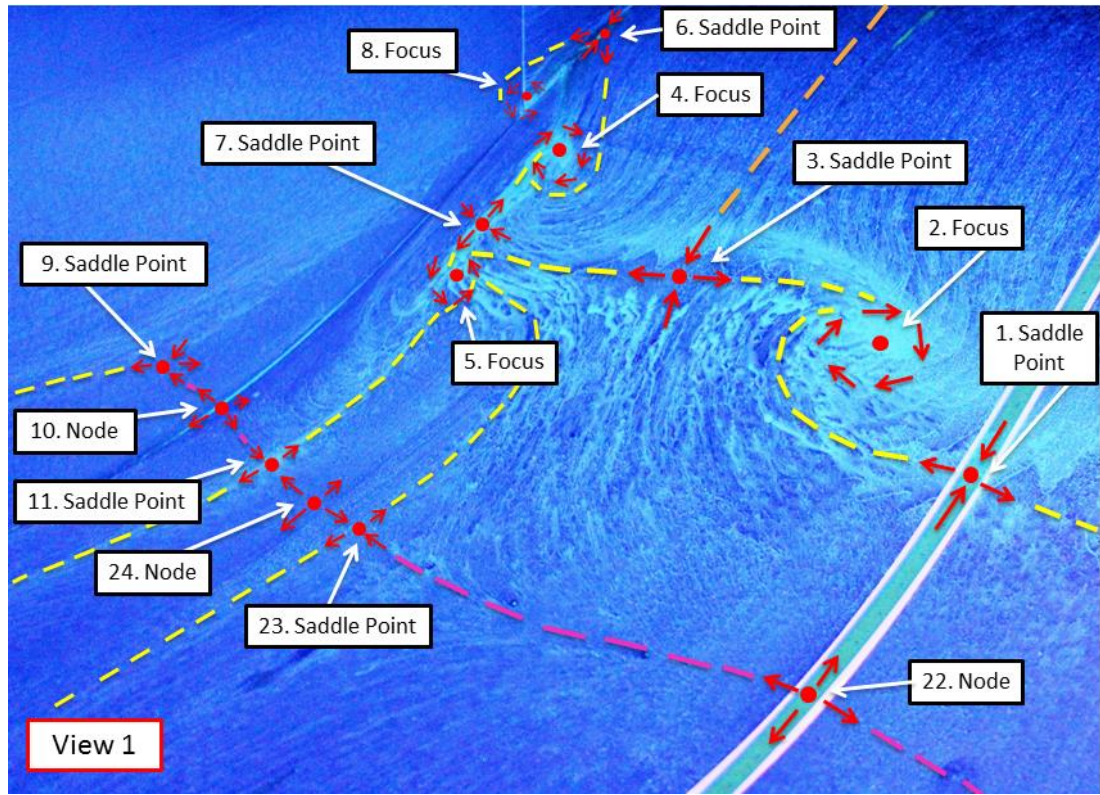
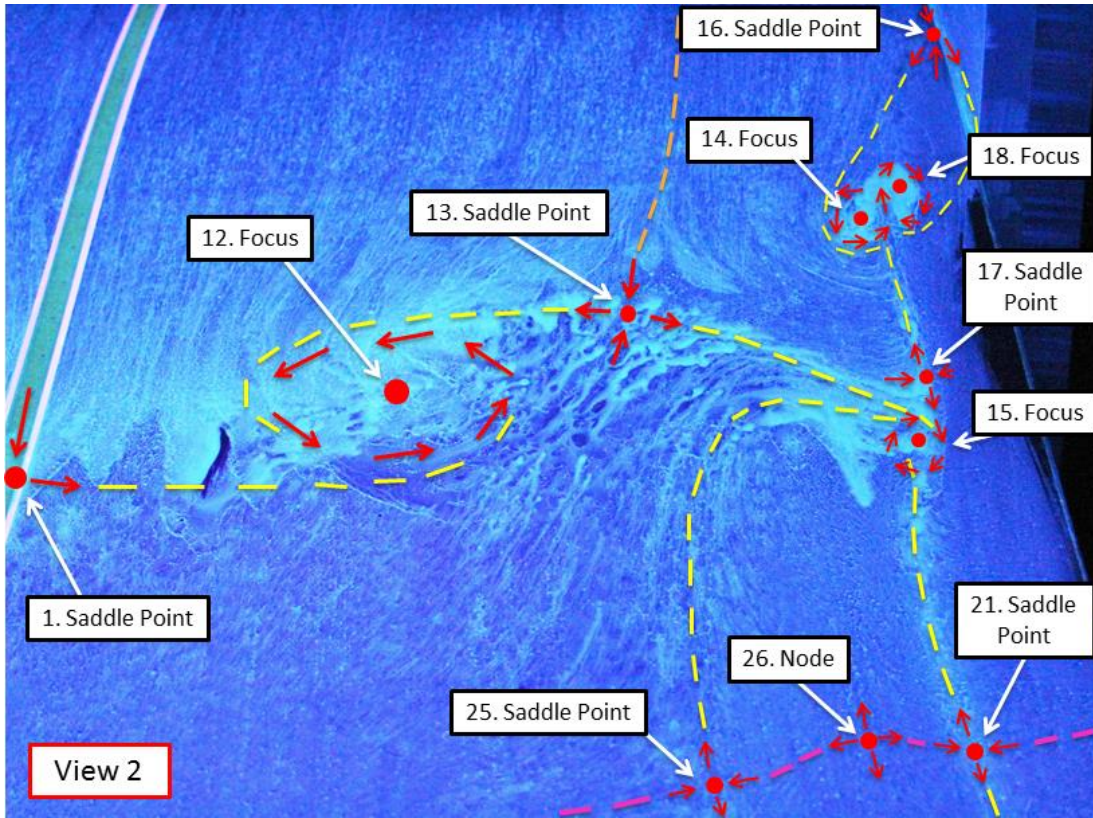


Figure 9 View 1, from Figure 4.7, highlighting the topological features on the far side (wind tunnel inner loop) with yellow dashed lines indicating separation, orange dashed lines showing the isolation of the near sidewall flow from the central flow separation,



*Figure 10 View 2, from Figure 4.7, highlighting the topological features on the near side (wind tunnel outer loop) with yellow dashed lines indicating separation, orange dashed lines showing how the near sidewall flow is topologically isolated from the central flow separation, and magenta dashed lines indicating reattachment. The incoming flow is from right to left.*

### Case C

The global surface flow pattern for the attached flow case, Case C, is shown in Figure 11. This is the simplest of the three cases because the only surface flow features remaining are due to the sidewall flow separation. In the central region of the ramp, the flow remains attached, in the mean sense, with a strong degree of side-to-side symmetry present. However, while the flow remains attached here, there is still evidence of a component of crossflow, directed from the central region of the ramp surface toward the tunnel sidewalls. Near both sidewalls, pockets of separation appear in the form of two saddle-foci pairs, one on each side.

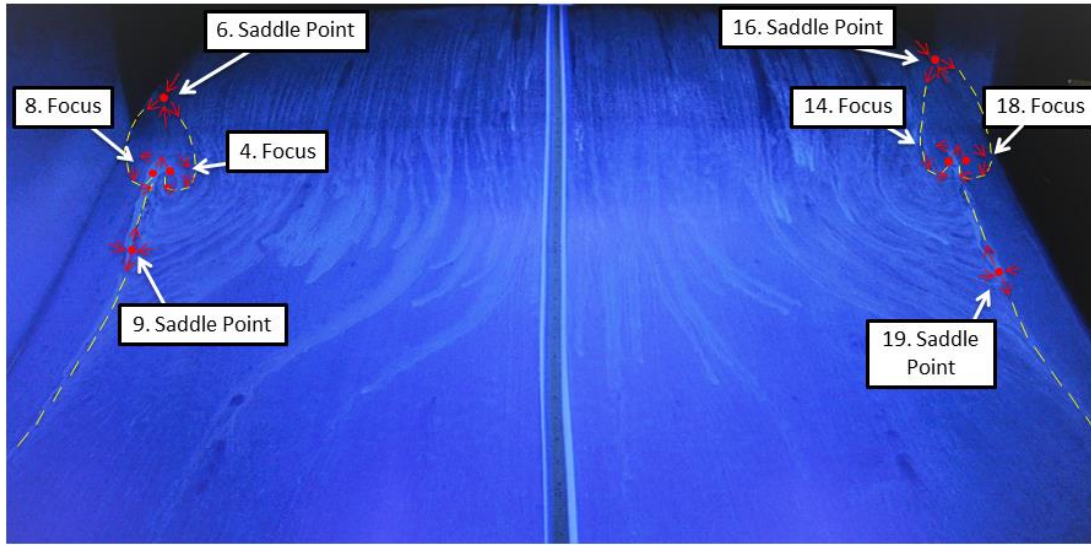


*Figure 11 Global surface flow visualization for the attached flow, Case C, highlighting the symmetric pockets of sidewall separation that remain. The incoming flow is from top to bottom.*

## References

- [1] Simmons, D., Thomas, F. O., and Corke, T. C. Smooth Body Flow Separation Experiments and Their Surface Flow Topology Characterization. Dallas, TX, 2019.
- [2] Simmons, D. J. *An Experimental Investigation of Smooth-Body Flow Separation*. Ph.D. Thesis. University of Notre Dame, Notre Dame, Indiana, 2020.
- [3] Koklu, M., and Owens, L. R. "Comparison of Sweeping Jet Actuators with Different Flow-Control Techniques for Flow-Separation Control." *AIAA Journal*, Vol. 55, No. 3, 2017, pp. 848–860. <https://doi.org/10.2514/1.J055286>.
- [4] Tobak, M., and Peake, and D. J. "Topology of Three-Dimensional Separated Flows." *Annual Review of Fluid Mechanics*, Vol. 14, No. 1, 1982, pp. 61–85. <https://doi.org/10.1146/annurev.fl.14.010182.000425>.

Appendix – Case A

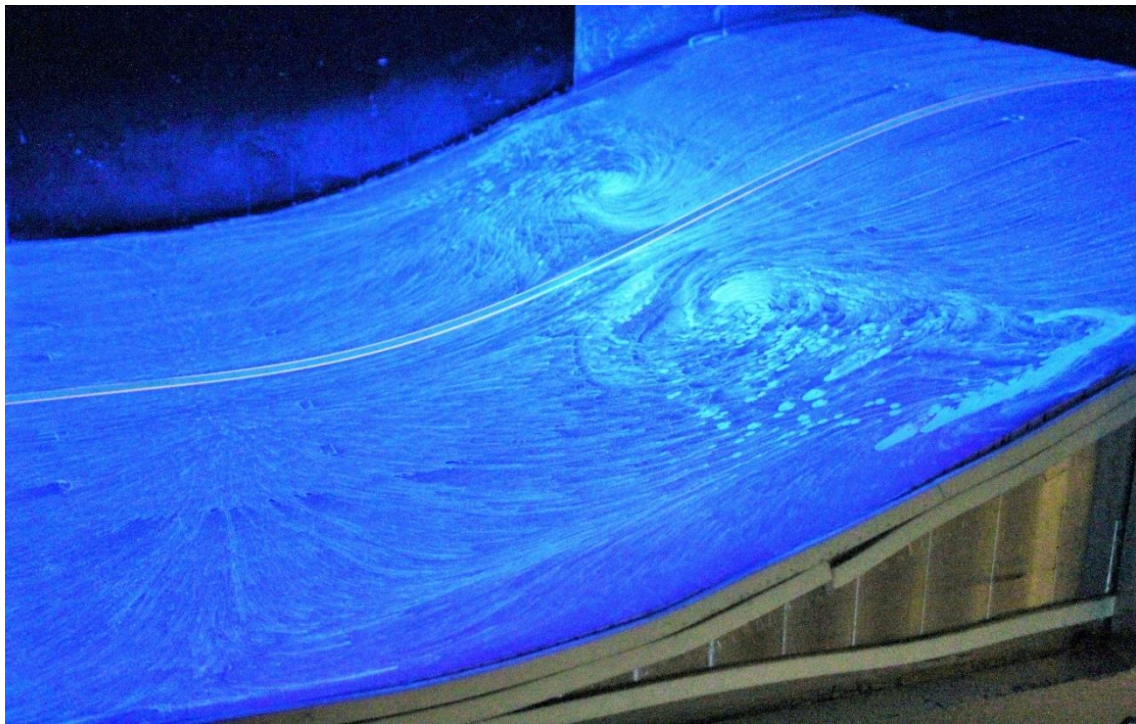


*Figure 12 Surface flow visualization for Case A with incoming flow from right to left (Test 32, February 2018)*

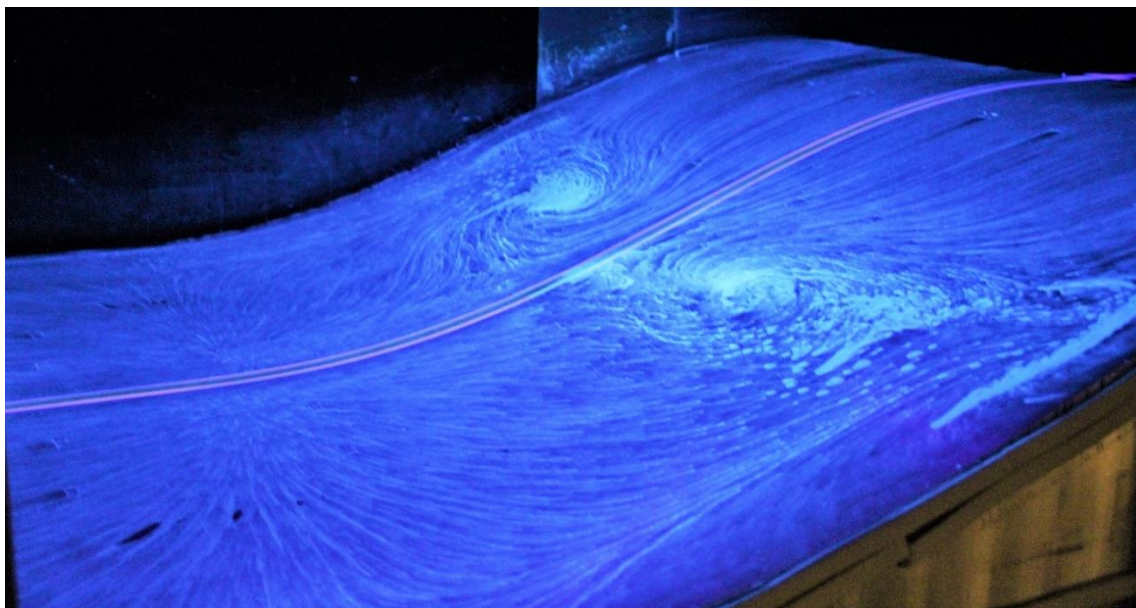


*Figure 13 Surface flow visualization for Case A with incoming flow from right to left (Test 21, February 2018)*

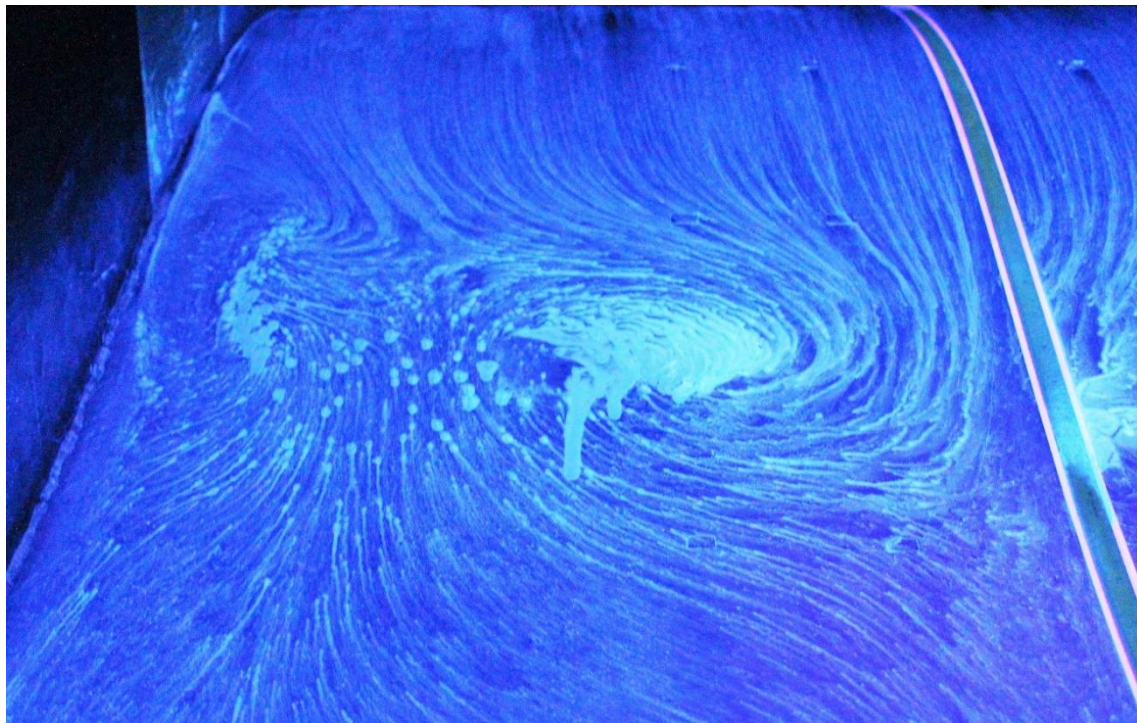


Figure 14 Surface flow visualization for Case A with incoming flow from top to bottom (Test 21, February 2018)

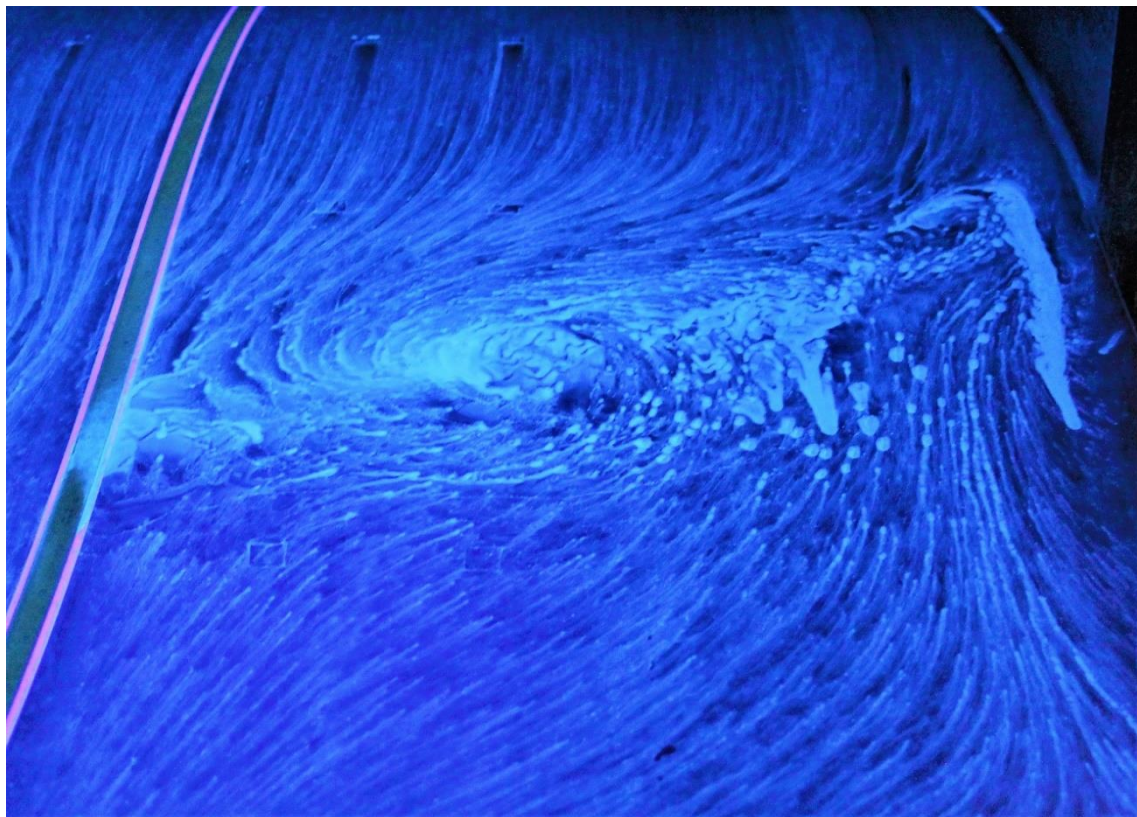


Figure 15 Surface flow visualization for Case A with incoming flow from top to bottom (Test 21, February 2018)

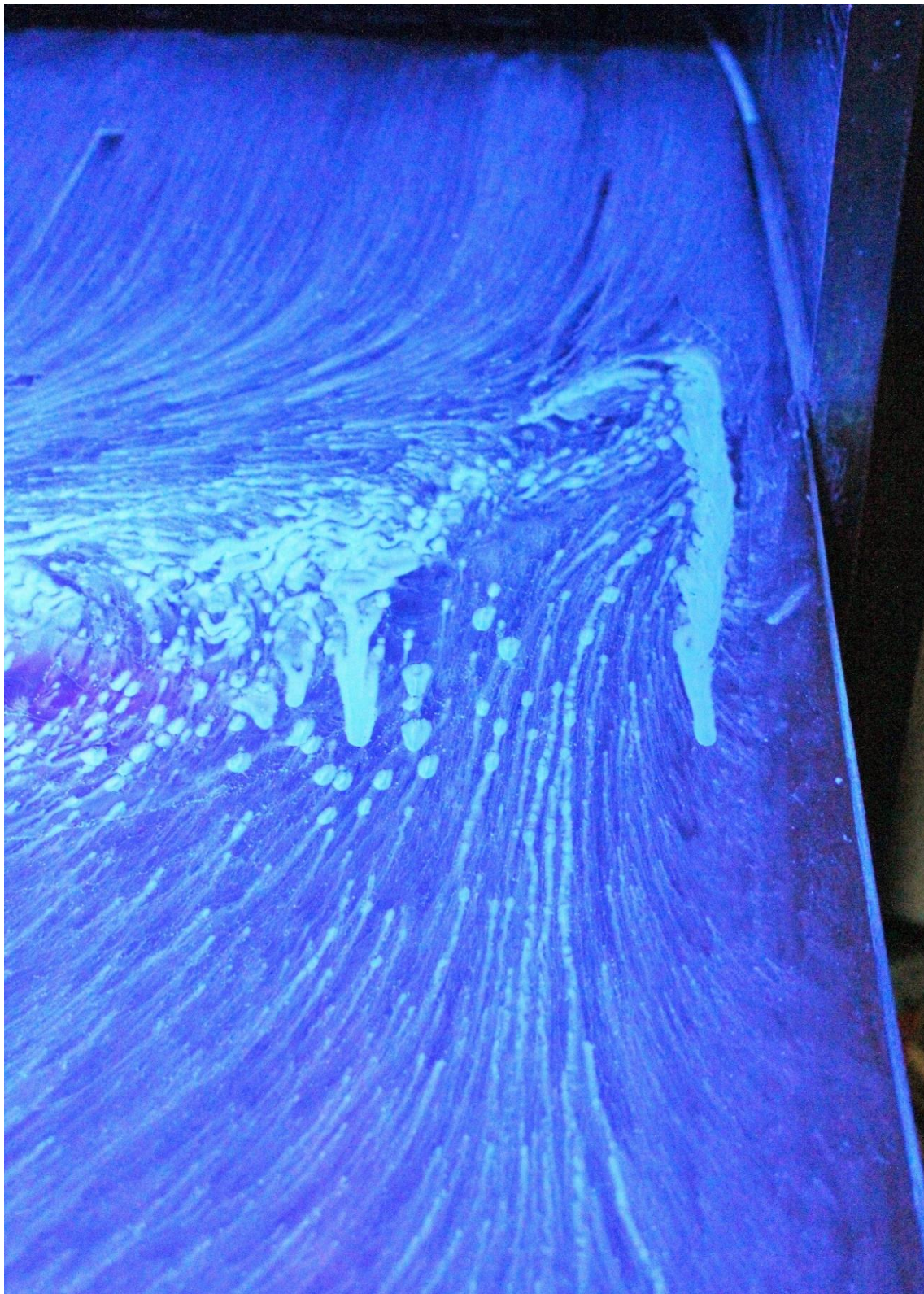


Figure 16 Surface flow visualization for Case A with incoming flow from top to bottom (Test 21, February 2018)

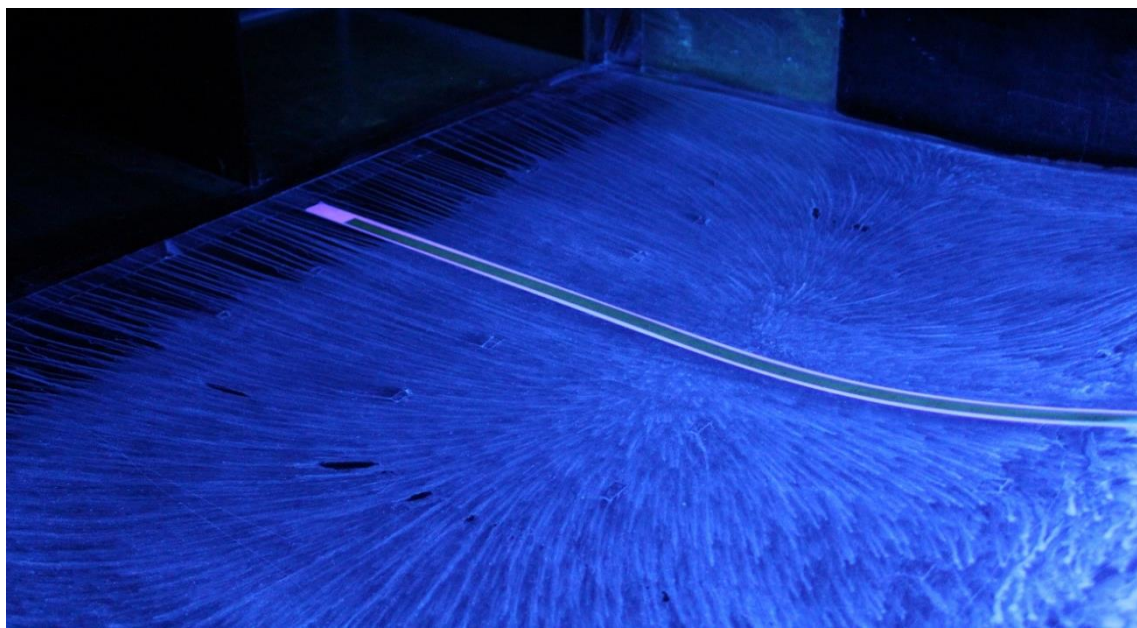


Figure 17 Surface flow visualization for Case A with incoming flow from right to left (Test 21, February 2018)

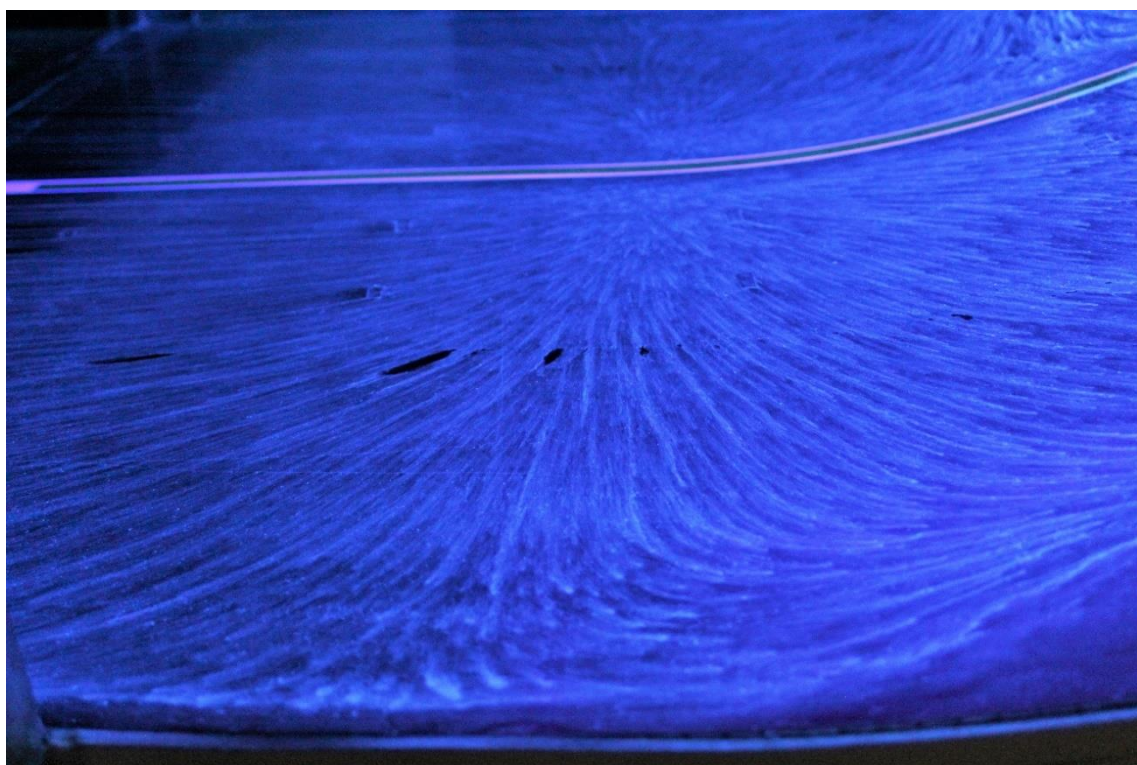
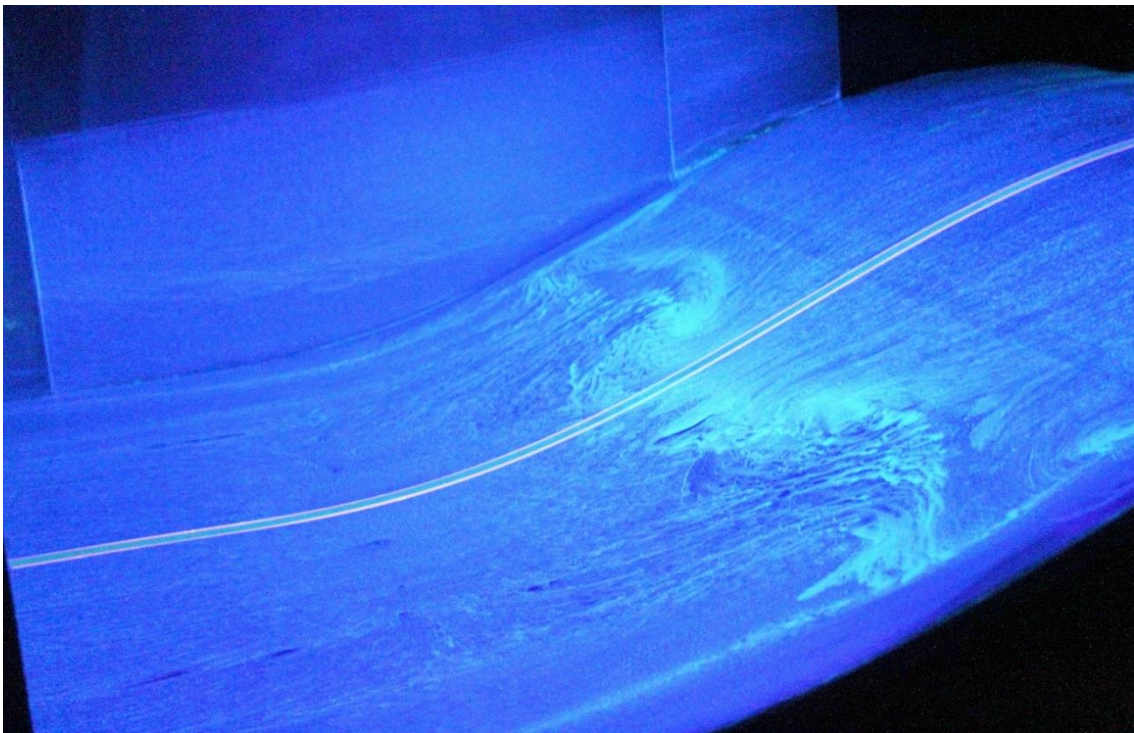
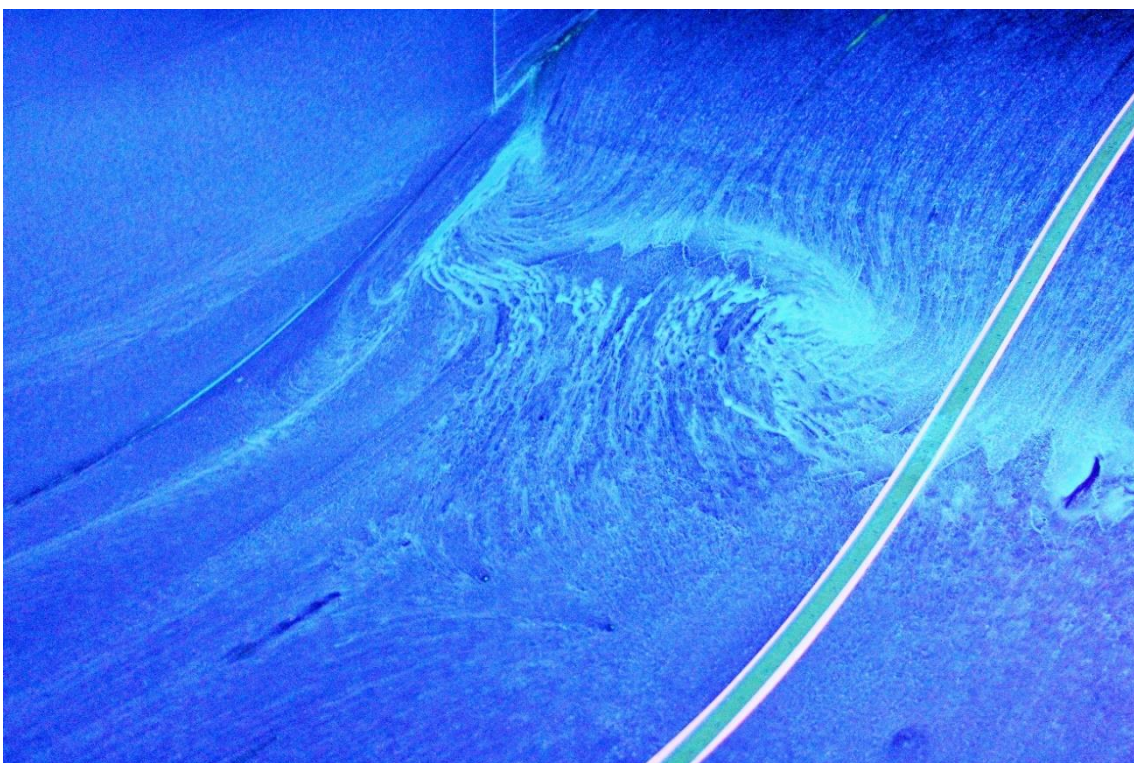


Figure 18 Surface flow visualization for Case A with incoming flow from right to left (Test 21, February 2018)

Appendix – Case B



*Figure 19 Surface flow visualization for Case B with incoming flow from right to left (Test 1, January 2019)*



*Figure 20 Surface flow visualization for Case B with incoming flow from right to left (Test 1, January 2019)*

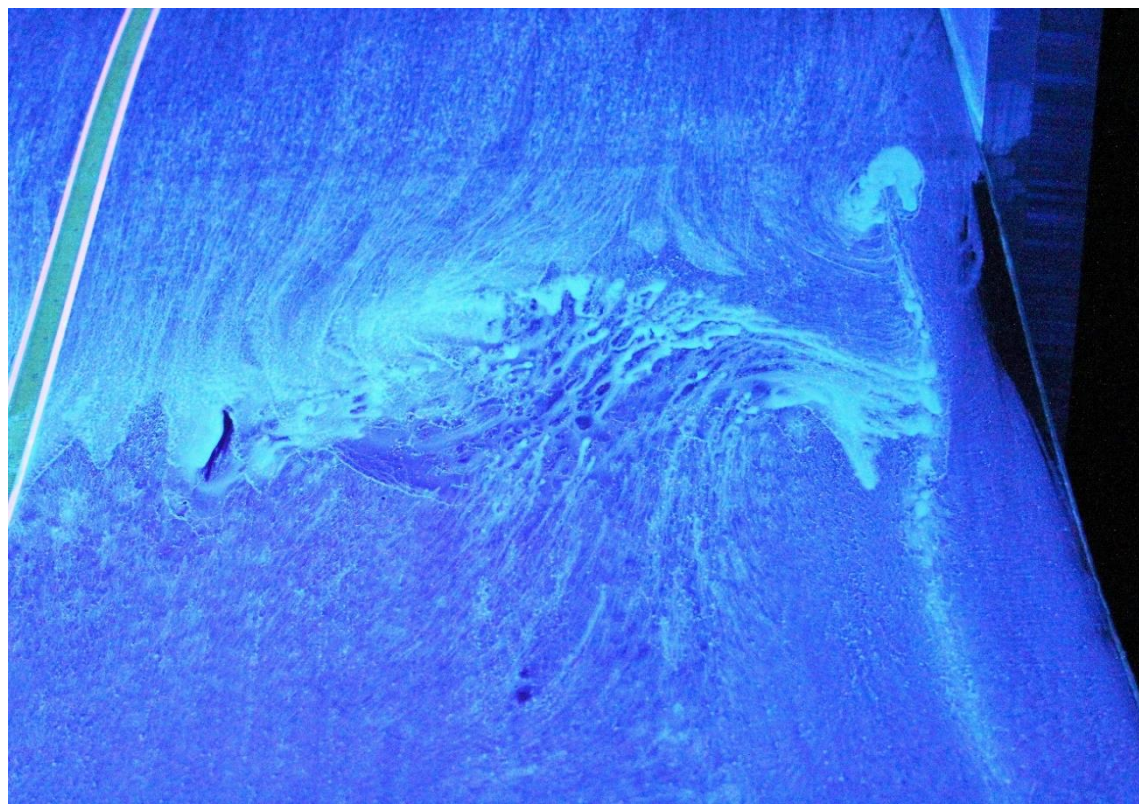


Figure 21 Surface flow visualization for Case B with incoming flow from top to bottom (Test 1, January 2019)

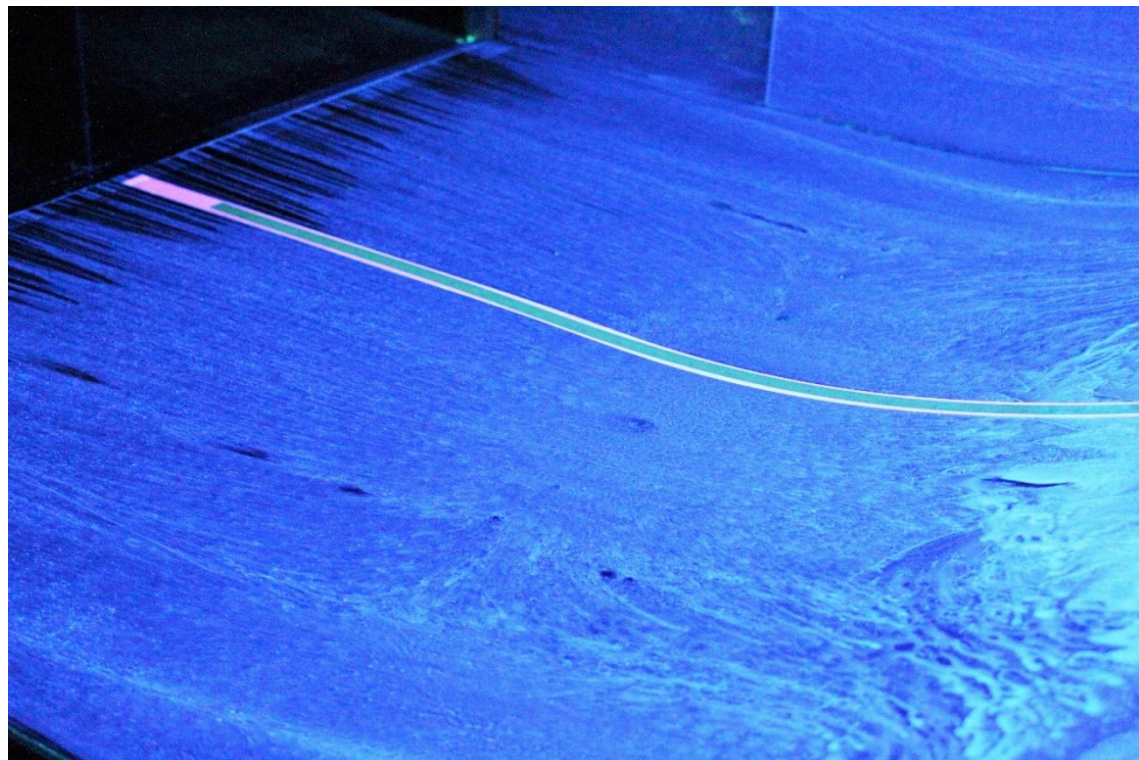


Figure 22 Surface flow visualization for Case B with incoming flow from right to left (Test 1, January 2019)

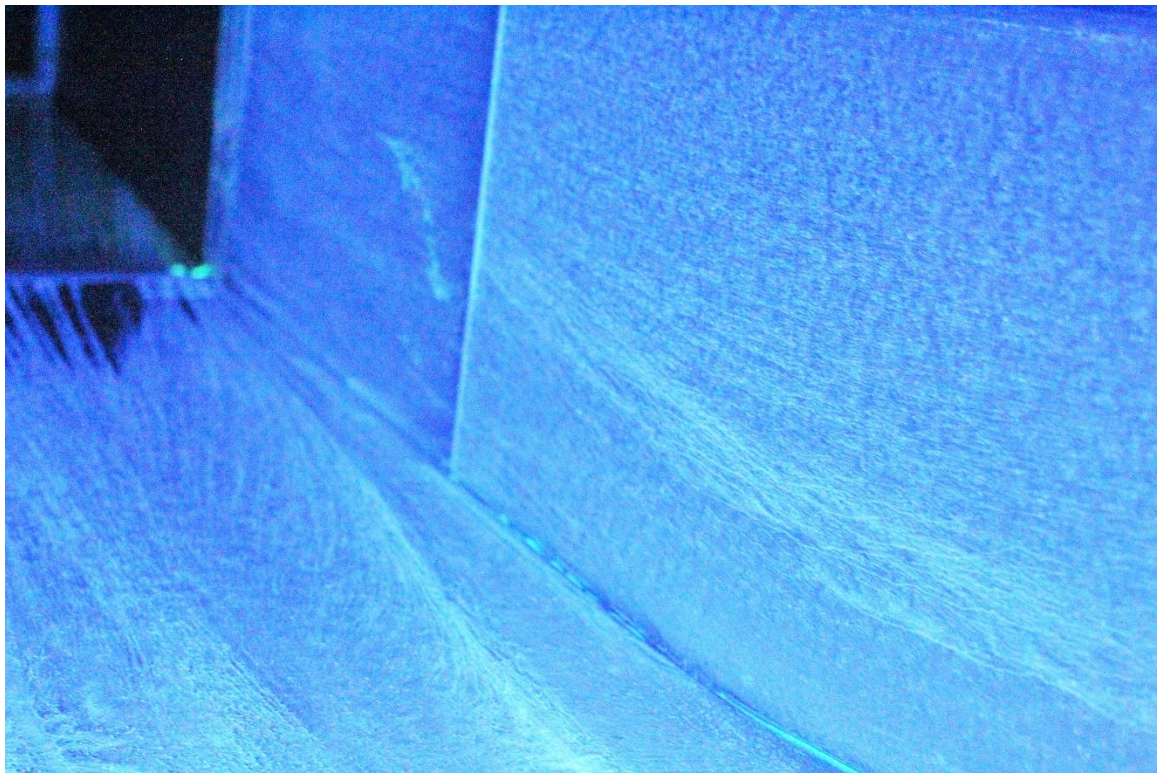


Figure 23 Surface flow visualization for Case B with incoming flow from right to left (Test 1, January 2019)

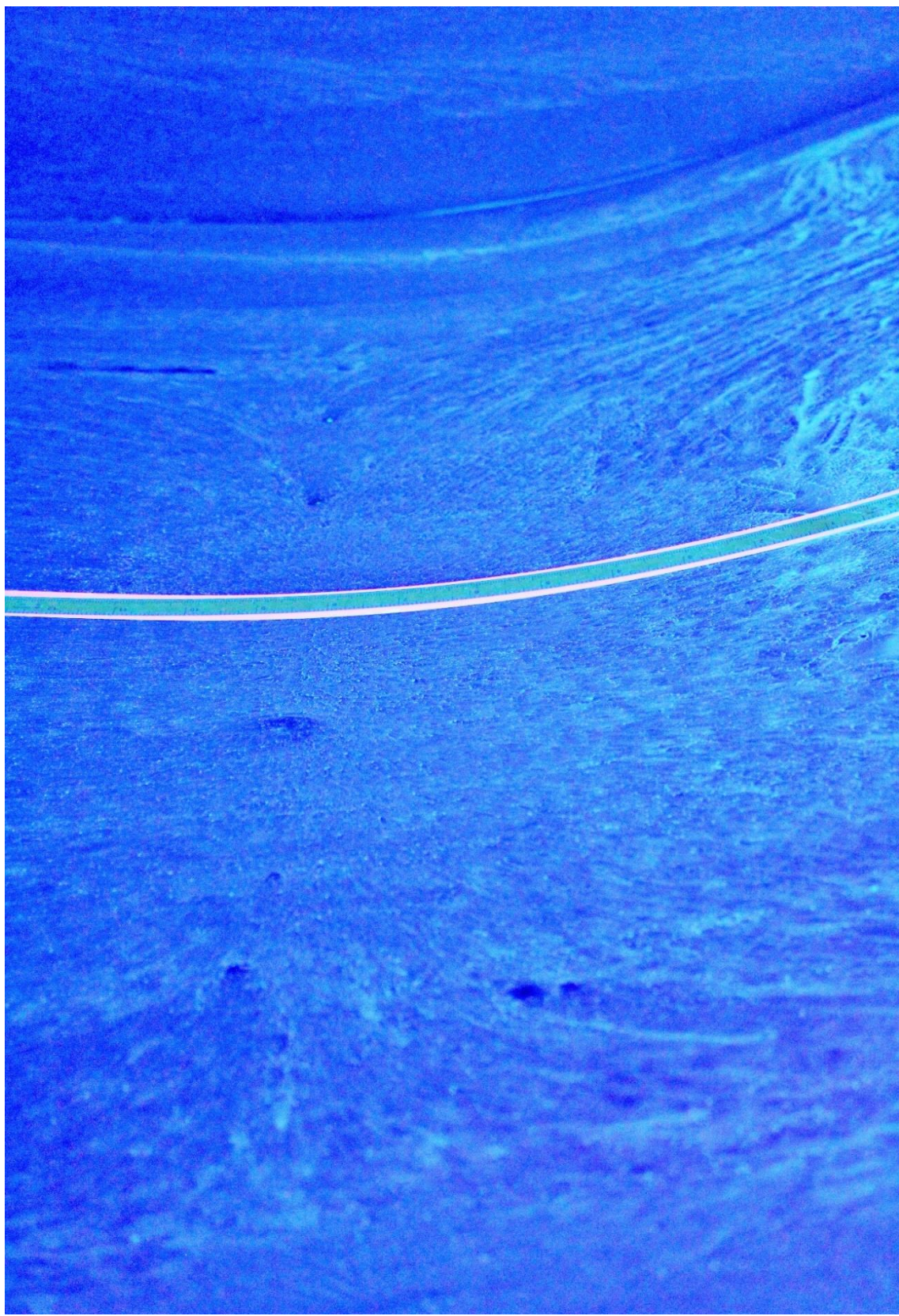


Figure 24 Surface flow visualization for Case B with incoming flow from right to left (Test 1, January 2019)

## Appendix – Case C

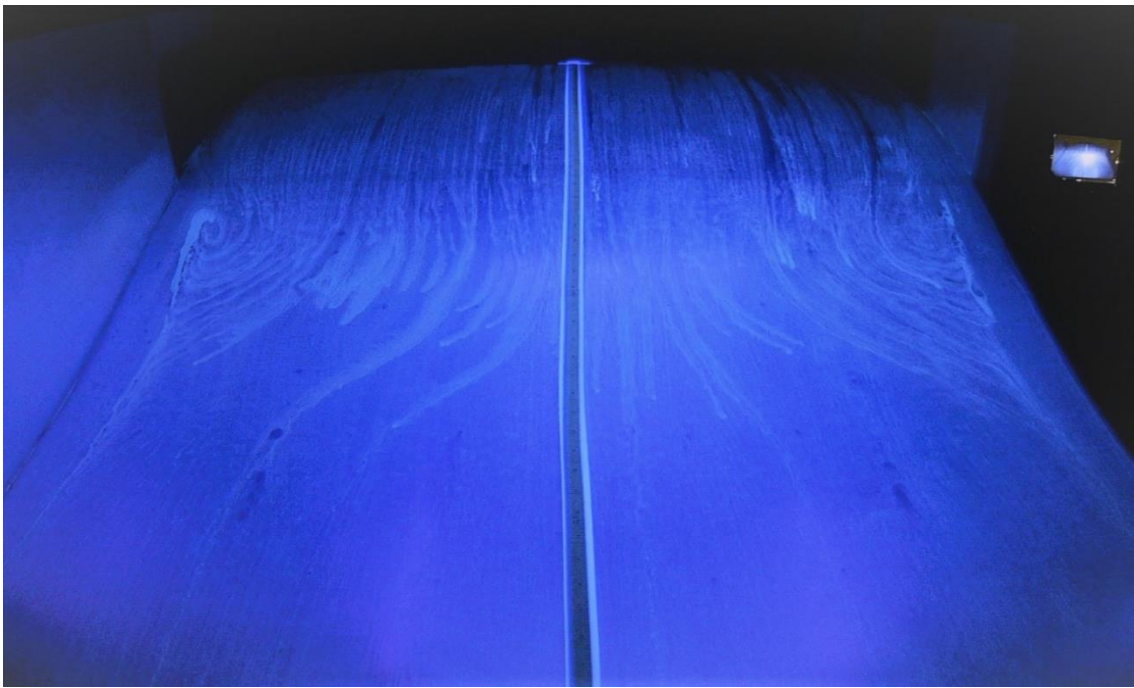


Figure 25 Surface flow visualization for Case C with incoming flow from top to bottom (Test 1, July 2019)

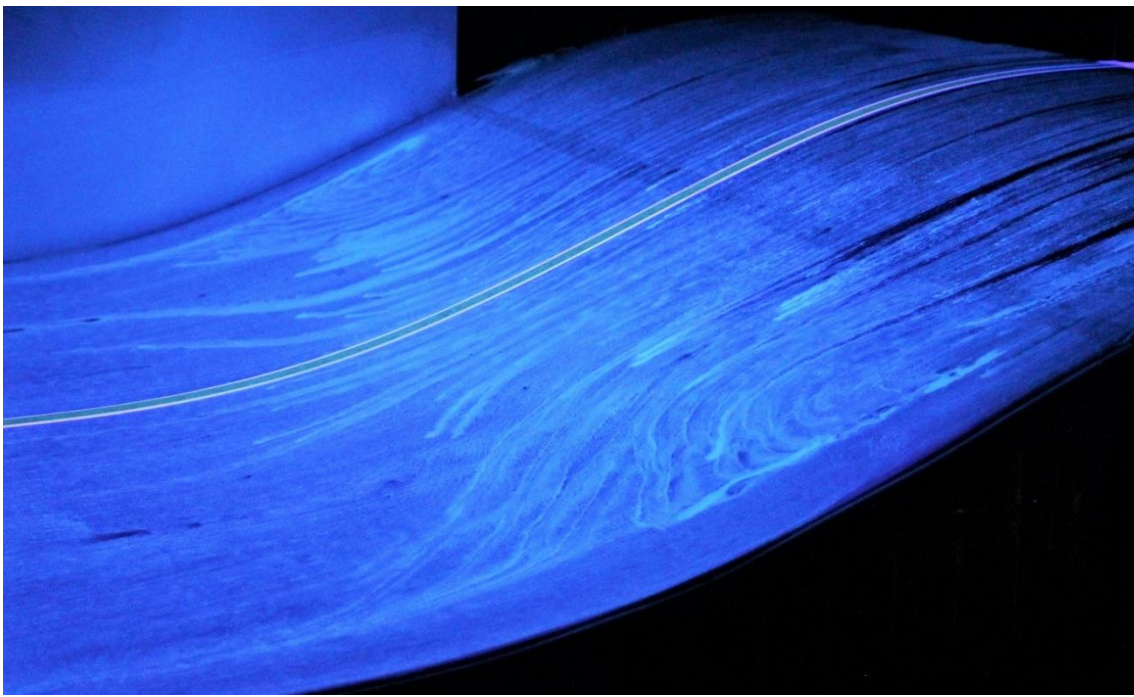


Figure 26 Surface flow visualization for Case C with incoming flow from right to left (Test 1, July 2019)

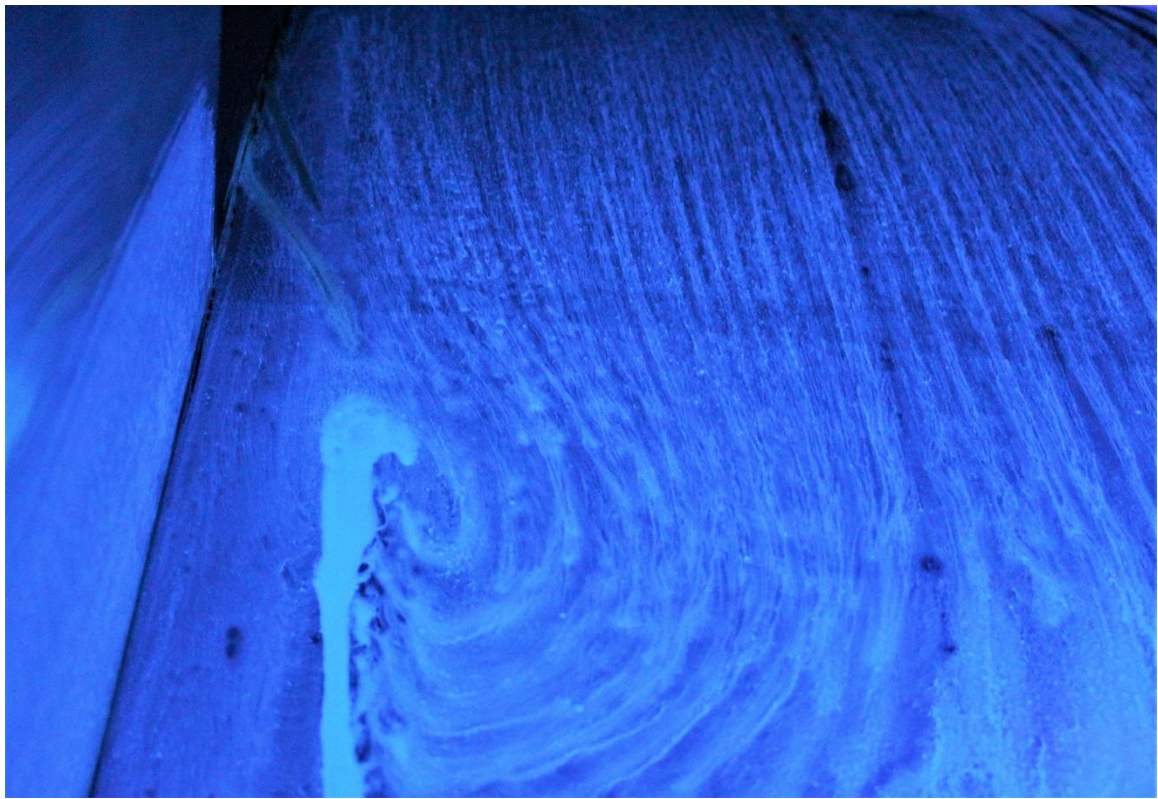


Figure 27 Surface flow visualization for Case C with incoming flow from top to bottom (Test 1, July 2019)